





SIMULTANEOUS SPARSE DECONVOLUTION

Erick Costa e Silva Talarico ^{*}, Matheus Cafaro Arouca Sobreira ,
Andre Gomes de Araujo , Carlos Alves da Cunha Filho 

Petrobras – Petróleo Brasileiro S.A, Rio de Janeiro, RJ, Brazil

*Corresponding author email: erick.talarico@petrobras.com.br

ABSTRACT. Increasing seismic resolution has been long pursued by the geophysical community, serving, among other applications, for more detailed interpretation of seismic clinofolds, better seismic inversion and quantitative interpretation. Sparse deconvolution methods play a central role in this pursuit. However, although sparse methods have performed well for single seismic stack or acoustic inversion tasks, their application for multi-stack seismic volumes and consequent use in elastic inversion are still a challenging and ongoing research topic. The challenge is to obtain reflectivity volumes with high correlation between them. In this study, we present a new method to perform simultaneous sparse deconvolution (SSD) in a group of seismic volumes associated with different reflection angles. The proposed algorithm enforces co-localization of the spikes on the estimated reflectivity traces and additionally allows user control of the sparsity via hyperparameters. The method is validated in both synthetic and real datasets proving its co-localization capability and resulting in higher correlations between the reflectivity volumes, when compared to independent sparse deconvolution (ISD) of the seismic stacks. The resulting reflectivity volumes are, henceforth, better suited for downstream tasks such as high-resolution amplitude versus angle (AVA) analysis or input for high-resolution elastic inversions.

Keywords: partial stacks; amplitude versus angle; sparsity; deconvolution.

INTRODUCTION

The band-limited character of routine seismic image volumes imposes resolution constraints (limited separability of two adjacent events in the seismic signal) for hydrocarbon reservoir characterization. These constraints are particularly restrictive for depositional settings with complex stratigraphic features.

According to [Sheriff \(1991\)](#), deconvolution is a data processing technique applied to seismic reflection and other data for the purpose of improving the recognizability and resolution of reflected events. There are many types of deconvolution methods in the literature, and [Rosa \(2018\)](#) describes some of them. Based on the assumption that the subsurface rocks are mainly composed of layers with sharp interfaces, sparse spike deconvolution methods (sparse meaning a time series with limited number of non-zero elements) extend

the spectral bandwidth of these seismic volumes, thus improving the resolution of heterogeneous stratigraphic features ([Hargreaves et al., 2013](#); [Kazemi and Sacchi, 2014](#); [Rosa, 2018](#)). The general goal of these methods is to transform the seismic traces in an estimate of the reflection coefficient series associated with the geological layer interfaces.

Acoustic inversion methods can also benefit from the bandwidth extension provided by sparse spike deconvolved data, by using it as input to the inversion algorithm ([Cunha et al., 2019](#)).

In order to extend the applicability of sparse spike deconvolution to elastic inversion, it is advisable to constraint the solutions from traces associated with the same spatial position and different reflection angles, so that the reflectivities from different angle stacks are

representative of the same geological interfaces. [Xi et al. \(2018\)](#) solve the problem by using a multivariate version of a modified Cauchy distribution. But, unlike the solution presented in this paper, the modified Cauchy distribution in [Xi et al. \(2018\)](#) has no parameter to control the sparsity (amount of zero coefficients in the reflectivity series) of the solution and does not develop the full posterior distribution over the reflectivities.

Our work is based on the Automatic Relevance Determination (ARD) formalism explained in [Bishop \(2006\)](#). This is a fully Bayesian formalism which was created for linear regression problems, where one is interested in finding the sparsest solution (solution with a minimal number of non-zero coefficients), but it can be applied to any linear inverse problem. In the geophysics literature, there are few publications that explore ARD formalism: [Valentine and Sambridge \(2018\)](#) present it in the context of inversion regularization techniques; [Ji et al. \(2020\)](#) apply ARD to amplitude versus angle (AVA) joint inversion to P and S reflectivities.

The novelty of the present work is that we apply the ARD algorithm to AVA inversion with a different kind of prior than the one used in [Ji et al. \(2020\)](#), which enforces the co-localization of the reflectivity spikes throughout the different reflectivity traces. The present paper also makes no assumption regarding the seismic error spatial structure, which is determined in the proposed optimization algorithm.

The results presented in this paper discuss the problem of deconvolution of seismic partial stacks, although the tools developed here could also be applied to any kind of AVA seismic inversion (such as AVA to elastic reflectivity inversion, for example).

THEORY

ARD applied to Geophysics

Many geophysical problems may be cast into or approximated by a linear system, with Gaussian noise. For example, given an input vector r and an output vector s , with the linear transformation G , one can write:

$$\begin{aligned} s &= Gr + \epsilon \\ \epsilon &\sim \mathcal{N}(\epsilon|0, S), \end{aligned} \quad (1)$$

where S is the covariance matrix of the measurement noise and is usually assumed to be diagonal and uniform (independent and identically distributed noise). In this work, we will make no such assumption.

For seismic 1D convolutional model, the matrix G is a given Toeplitz matrix, which represents the convolution of the input reflectivity trace r with the estimated seismic wavelet. The prior probability over r is defined by:

$$p(r) = \mathcal{N}(r|0, A^{-1}) \quad (2)$$

The ARD assumption is that the prior precision matrix A is diagonal, with independent entries:

$$\begin{aligned} A &= \begin{bmatrix} \lambda_1 & 0 & \dots & 0 \\ 0 & \lambda_2 & \dots & 0 \\ \dots & \dots & \dots & \dots \\ 0 & 0 & \dots & \lambda_N \end{bmatrix} \\ &= \text{diag}(\lambda_1, \lambda_2, \dots, \lambda_N) \\ &= \text{diag}(\lambda) \end{aligned} \quad (3)$$

In a maximum a posteriori (MAP) approach, one is interested in finding the vector r which maximizes the posterior probability $p(r|s, \lambda, S)$:

$$p(r|s, \lambda, S) = \frac{p(s|r, S)p(r|\lambda)}{p(s|\lambda, S)} \quad (4)$$

The above maximization problem is equivalent to minimizing the loss:

$$U(r) = (s - Gr)^T S^{-1} (s - Gr) + \sum_{j=1}^N \lambda_j r_j^2, \quad (5)$$

which is equivalent to a deterministic inversion with regularization term. In this setting, the best choice of λ from the mismatch point of view is zero (the smaller the regularization, the better is the match between measured s and simulated Gr). On the other hand, the smaller mismatch usually comes at the expense of unstable (noisier) solutions. [Figure 1](#) illustrates this situation for a 2D toy example. The Bayesian approach brings a natural way of finding the optimal value of the regularization hyperparameters λ that balances mismatch and solution quality.

In a fully Bayesian approach, one is interested in characterizing the posterior distribution $p(r|s, \lambda, S)$; in this context, the optimal parameters (λ, S) are obtained by maximizing the marginal likelihood $p(s|\lambda, S)$:

$$p(s|\lambda, S) = \int_r p(s|r, S)p(r|\lambda) dr \quad (6)$$

The above integral can be regarded as an inner product of the functions $f_s(r) = p(s|r, S)$ and $g_\lambda(r) = p(r|\lambda)$. For a fixed seismic error matrix S , the maximum

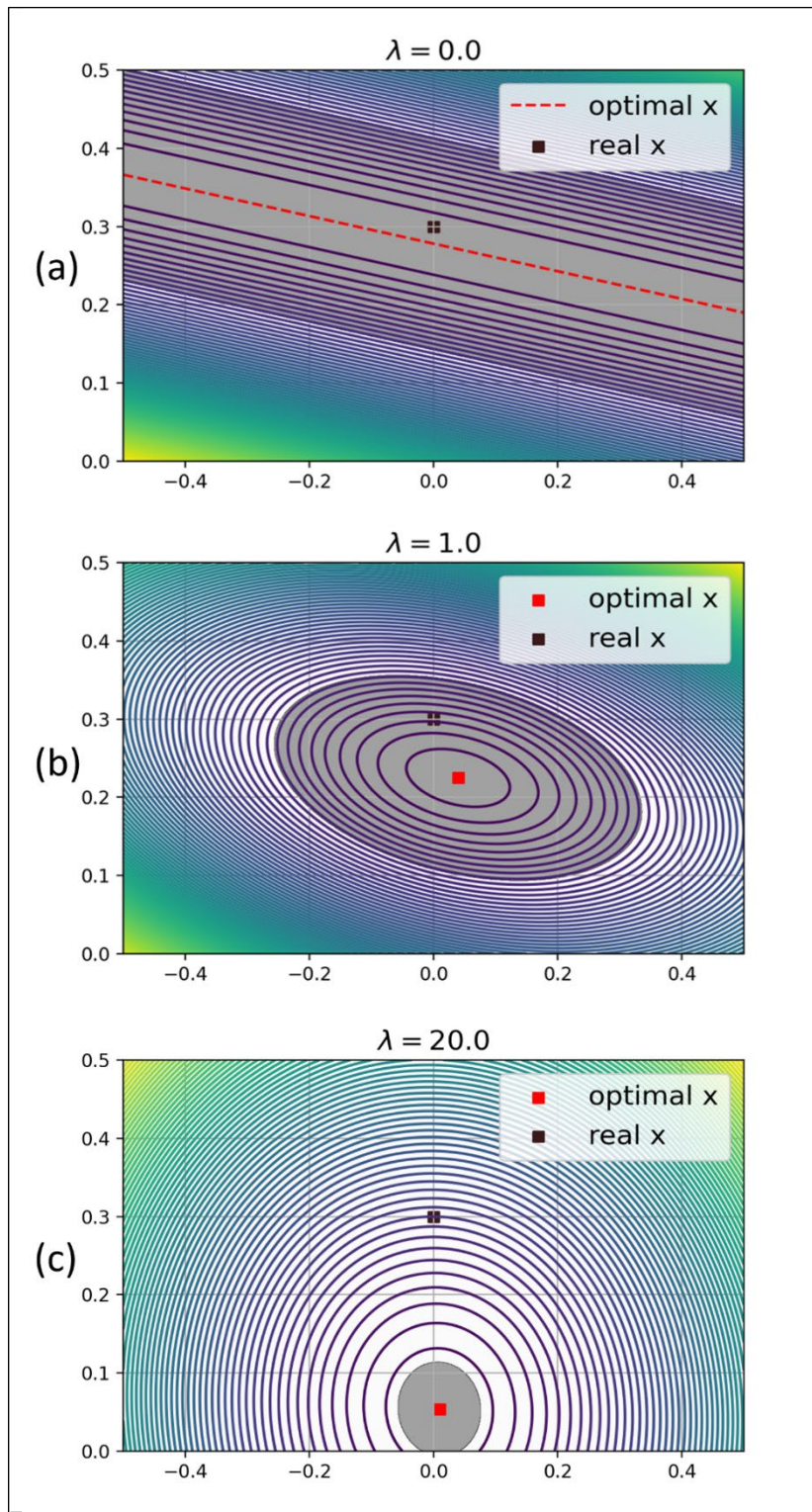


Figure 1: Bayesian inversion applied to a 2D toy example for different values of the hyperparameter $\lambda_1=\lambda_2=0$. (a), 1.0 (b), and 20.0 (c). The matrix G is singular, so when $\lambda_1=\lambda_2=0$ there are infinite optimal solutions.

marginal likelihood is achieved by finding the vector λ , which maximizes the projection of $g_\lambda(r)$ over $f_S(r)$. This is neither achieved with $\lambda \approx \vec{0}$ (equiprobable distribution over r) nor with $\lambda \rightarrow \infty$ (distribution of r peaked at the solution $r = \vec{0}$); but there is an optimal non-trivial solution.

The above integral is not analytical to be computed and its derivatives are also not analytical (besides, they suffer from vanishing gradients). For this reason, one can use the identity below, which holds for any test distribution $q(r)$:

$$\begin{aligned} \log p(s|\lambda, S) &= \mathcal{L}(q, \lambda, S) \\ &+ D_{KL}(q(r)|p(r|s, \lambda, S)) \\ &\geq (q, \lambda, S) \end{aligned} \quad (7)$$

$$\mathcal{L}(q, \lambda, S) = \mathbb{E}_{q(r)} \left[\log \frac{p(s, r|\lambda, S)}{q(r)} \right] \quad (8)$$

$$\begin{aligned} D_{KL}(q(r)|p(r|s, \lambda, S)) \\ = \mathbb{E}_{q(r)} \left[\log \frac{q(r)}{p(r|s, \lambda, S)} \right] \end{aligned} \quad (9)$$

The D_{KL} is the Kullback-Leibler divergence and measures the discrepancy between the proposed distribution $q(r)$ and the true posterior $p(r|s, \lambda, S)$. It is always greater than or equal to zero; equality only holds when $q(r) \equiv p(r|s, \lambda, S)$.

The $\mathcal{L}(q, \lambda, S)$ term is known as Evidence Lower Bound and maximizing it with respect to q is equivalent to minimizing the D_{KL} term. The EM algorithm (Expectation Maximization) consists of optimizing the marginal likelihood $p(s|\lambda, S)$ by alternating two optimization steps. It can be described in the Algorithm 1:

<p>Input: seismic trace s, number of iterations n_{iter} Output: optimum reflectivity precisions $\lambda = (\lambda_1, \lambda_2, \dots, \lambda_N)$ and measurement error covariance matrix S</p>
<p>1 Initialize λ_0 and S_0 2 for $i = 1$ to n_{iter} do 3 E-step: set the test distribution $q(r) = p(r s, \lambda_0, S_0)$ 4 M-step: maximize the ELBO $\mathcal{L}(q, \lambda, S)$ in relation to λ and S, fixing $q(r) = p(r s, \lambda_0, S_0)$ 5 set $\lambda_0 = \lambda$ and $S_0 = S$ 6 set $\lambda_0 = \lambda$ and $S_0 = S$ 7 end</p>

Algorithm 1: Expectation Maximization (EM) algorithm for maximizing the marginal likelihood probability.

The posterior distribution of the E-step is developed in [Buland and Omre \(2003\)](#), and can be written as:

$$\begin{aligned} p(r|s, \lambda_0, S_0) &= \mathcal{N}(r|\hat{r}, \Lambda_r^{-1}) \\ \hat{r} &= \Lambda_r^{-1} G^T S_0^{-1} s \\ \Lambda_r &= A_0 + G^T S_0^{-1} G \end{aligned} \quad (10)$$

In the M-step, one can ignore the terms which do not depend on λ or S :

$$\begin{aligned} \lambda, S &= \operatorname{argmax}_{\lambda, S} \mathbb{E}_{q(r)} [\log p(s, r|\lambda, S)] \\ &= \operatorname{argmax}_{\lambda, S} \int_r p(r|s, \lambda_0, S_0) \log p(s, r|\lambda, S) \end{aligned} \quad (11)$$

The solution to the above optimization problem is given by:

$$\lambda_i = \frac{1}{[\Lambda_r^{-1}]_{i,i} + \hat{r}_i^2} = \frac{1}{\mathbb{E}[r_i^2]} \quad (12)$$

$$S = G \Lambda_r^{-1} G^T + (G \hat{r} - s)(G \hat{r} - s)^T \quad (13)$$

The above equations [10](#) through [13](#) are recursive equations since they have cyclic dependencies. The solution is found thus by iterative application of these equations.

Equation [13](#) comes from the assumption that seismic noise is distinguishable from the signal, which is not entirely true since noise and signal have similar frequency spectrum. For this reason, the estimate in Equation [13](#) may be rescaled at each iteration to match a desired signal to noise ratio (SNR), which can be parametrized by the seismic processing expert:

$$S_{scaled} = \gamma [G \Lambda_r^{-1} G^T + (G \hat{r} - s)(G \hat{r} - s)^T] = \gamma S \quad (14)$$

$$\begin{aligned} SNR &= \frac{P_{signal}}{P_{noise}} = \frac{P_{measured}}{P_{noise}} - 1 \\ &= \frac{s^T s}{\operatorname{tr}[S_{scaled}]} - 1 = \frac{s^T s}{\gamma \operatorname{tr}[S]} - 1 \end{aligned} \quad (15)$$

In the above equations, γ can be computed from the SNR and then it is used to compute the S_{scaled} matrix. As such, the signal to noise is a hyperparameter that indirectly controls the sparsity of the solution: for higher signal to noise ratio, the algorithm will try to match each and every seismic event, and the solution will be less sparse; for smaller signal to noise ratio, more events will be ignored by the algorithm, which will be able then to yield a sparser solution. This possibility to manually parametrize the sparsity of the solution is an advantage of the present method in comparison to the one of [Xi et al. \(2018\)](#), where such hyperparameter does not exist. Hyperparameter tuning can be used to find the SNR that yields the more geologically plausible result.

The EM algorithm tries to find the smallest values for the vector λ , and by doing that it induces sparsity in the solution (if consistent with the matrix G): the necessary entries of the vector r will be associated with smaller values λ_i , while the entries of r which can be set to zero, without compromising the measurement mismatch, will be associated with high λ_i values, and set to approximately zero after some iterations. [Figure 2](#) exemplifies the deconvolution of a seismic trace in the ARD formalism: the measured seismic equals the true seismic plus a colored noise; the ARD solution has a good visual match with the true reflectivity trace; it is sparser than the conventional deconvolution with similar seismic mismatch. [Figure 3](#) compares the estimated and actual seismic noise covariance functions and shows that they are similar.

ARD for multi-stack seismic deconvolution

In a multi-stack seismic deconvolution, the matrix G is a block-diagonal matrix, where each block is the Toeplitz matrix associated with the wavelet of the respective seismic stack. We would like to induce sparsity, without compromising the co-localization between the different reflectivity stacks, since they are generated from the same interface positions.

The way to do that is to elaborate more on the structure of the prior precision matrix A . Say, we choose A to be:

$$A = A_\theta \otimes A_t \quad (16)$$

$$A_\theta = \text{diag}(\lambda_{\theta 1}, \lambda_{\theta 2}, \dots, \lambda_{\theta F}) = \text{diag}(\lambda_\theta) \quad (17)$$

$$A_t = \text{diag}(\lambda_{t1}, \lambda_{t2}, \dots, \lambda_{tN}) = \text{diag}(\lambda_t), \quad (18)$$

where \otimes denotes the kronecker product (Lyche, 2020); F is the number of angle stacks; and N is the number of trace samples. The above equations mean that a sample at position i and reflectivity stack j has precision equal to $\lambda_{\theta j} \lambda_{ti}$. This means that the matrix A_θ controls the weight of each stack in the solution and is shared among all samples.

The EM algorithm, together with the above prior precision matrix assumption, is what we will refer to as the simultaneous sparse deconvolution (SSD) formalism. In the SSD formalism Equations 12 and 13 must be adapted into the following equations:

$$\lambda_{ti} = \frac{F}{\sum_{j=1}^F \mathbb{E}[r_{i,j}^2] \lambda_{\theta j}} \quad (19)$$

$$\lambda_{\theta j} = \frac{N}{\sum_{i=1}^N \mathbb{E}[r_{i,j}^2] \lambda_{ti}}, \quad (20)$$

where $\mathbb{E}[r_{i,j}^2]$ is the estimated second moment of the i^{th} sample of the j^{th} reflectivity stack.

Impact of SSD algorithm on AVA analysis

Since each reflectivity trace is important to explain its correspondent seismic stack trace, the optimized A_θ will not induce sparsity, since it would mean to zero a whole reflectivity trace. Most importantly, equations 16 through 18 imply that if a sample is not important to explain the output seismic gather, then $\lambda_{ti} \gg 1$ and, therefore, all stack reflectivities will have $\lambda_{\theta j} \lambda_{ti} \gg 1$, meaning that the sparsity will be shared across the different reflectivity stacks. The converse is not true: if one or more reflectivity coefficients at position i are important (non-zero), the algorithm does not induce the

other coefficients at the same position to be non-zero, since $\lambda_{\theta j} \lambda_{ti}$ will be small for every stack j , and thus small regularization will be applied. As a consequence, seismic events with AVA type 2 or with amplitude dimming are not harmed by the algorithm.

Finally, the regularization takes into account the square of the reflectivity coefficients; thus, the sign of the coefficients does not impact the loss function. As a consequence, seismic events with sign change across different stacks (AVA type 1 or 2, for example) are also not harmed by the algorithm.

RESULTS

We will show the application of the SSD formalism to both a synthetic and a real case example. The SSD formalism will be compared to the ARD approach independently applied to each seismic stack, which we will refer to as independent sparse deconvolution (ISD).

Synthetic case

We created a sparse reflectivity trace by sampling from a Gaussian-Bernoulli process (sampling a random white noise and multiplying it by a binary random trace with 0.1 probability to be equal to 1). We derived elastic reflectivity traces (P, S and density) proportional to this initial reference reflectivity and guided by linearized rock physics relations. The simulated seismic stacks correspond to the reflection angles of 0, 15 and 30 degrees (Near, Mid and Far, respectively), and their respective reflectivities were computed using the Aki-Richards equations. The wavelets were modelled (in order to resemble the same spectrum as the real seismic data used in the next section) as butterworth filters with the same low-cut ramp (5Hz-10Hz) but decreasing high-cut ramps: 50Hz-80Hz for the Near stack, 30Hz-50Hz for the Mid stack, and 20Hz-40Hz for the Far stack. A colored noise with the same power spectrum as the wavelets was added such that the signal to noise ratio equals 20.

Figure 4 shows the deconvolution results for both ISD and SSD formalisms. The ISD has no one-to-one correspondence between spikes across the different reflectivity stacks and no alignment is guaranteed, whereas the SSD has aligned spikes and a better match with the true reflectivities. In this synthetic example, there is no true residual moveout between the traces, and the misalignment is solely due to differences in the partial stacks' resolutions.

Since ARD is a fully Bayesian formalism, Figure 4 also illustrates the 80% confidence interval of the reflectivities for the SSD case.

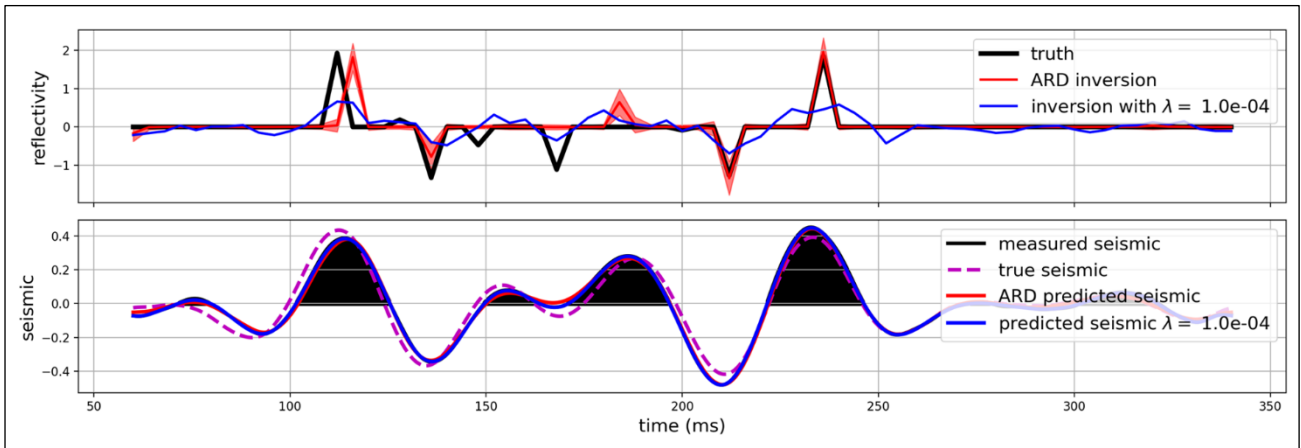


Figure 2: Application of the ARD formalism to deconvolve a seismic trace. It can be noted that the solution is sparse, and it has a good match with the measured seismic. An inversion with $\lambda_1=\lambda_2=\dots=\lambda_N=10^{-4}$ resulted in a not sparse solution with the same mismatch level.

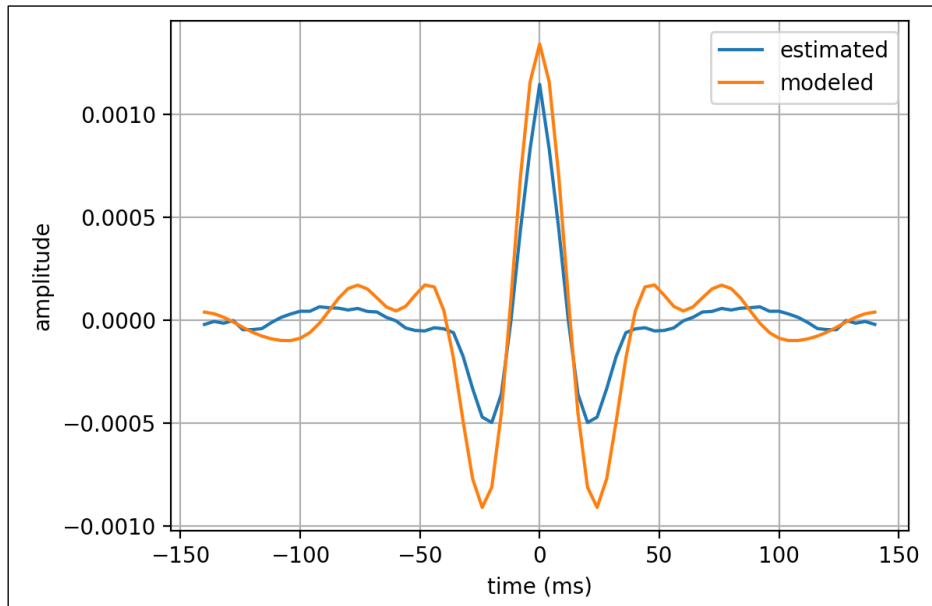


Figure 3: Covariance function of the seismic noise as a function of time lag. There is a good visual match between the estimated and modeled error structures.

Real Case

The real case example was taken from an offshore seismic, where a turbidite play was studied. The wavelets were calibrated from nearby wells (although statistical wavelets could also be used). The seismic stacks have sampling rate of 1ms and correspond to the following angle stacks: Near (2 to 12 degrees), Mid (10 to 22 degrees), Far (20 to 33 degrees), and Ultra Far (30 to 42 degrees). The signal to noise ratio hyperparameters were adjusted as 5, 5, 2, 1 for the Near, Mid, Far and Ultra Far stacks, in order

to achieve the best visual deconvolution results (alternatively, those values can be estimated from seismic to well tie), meaning that the Far and Ultra Far stacks are much more deteriorated by noise than the Near and Mid.

A first comparison between the ISD and SSD approaches is illustrated in [Table 1](#), which presents the correlations between different reflectivity stacks, showing that the SSD method results in higher correlations between the stacks.

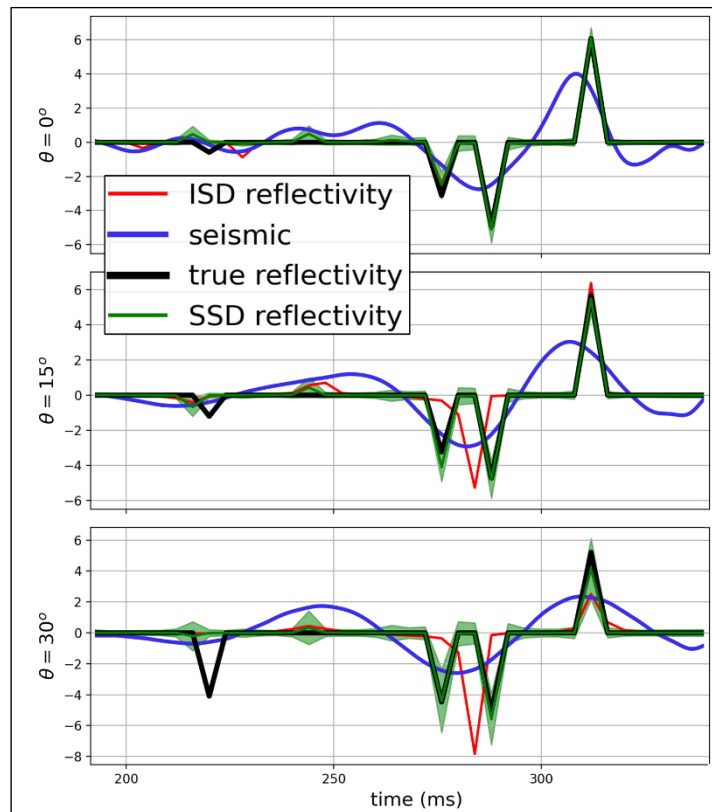


Figure 4: Comparison of ISD and SSD results. Each plot represents the deconvolution of a seismic stack (0, 15 and 30 degrees, respectively from top to bottom). The independent deconvolution (red traces) shows no one-to-one correspondence between the spikes across the different stacks, and no alignment is guaranteed. The simultaneous deconvolution (green traces) shows better correlation between spikes in different stacks, and better match with the true reflectivity traces. For the SSD case, the 80% confidence interval is also displayed.

Table 1: Correlation coefficients between the different reflectivity stacks for the SSD (green) and for the ISD (orange) cases. It can be noticed that the SSD correlation coefficients tend to have higher values.

	Near	Mid	Far	Ultra Far
Near		0.782	-0.043	-0.003
Mid	0.339		0.480	0.150
Far	0.111	0.188		0.448
Ultra Far	0.015	0.038	0.118	

Figure 5 compares the deconvolution results for a random trace within the seismic volume. It visually confirms that the SSD approach yields more aligned reflectivity traces.

The visual analysis of the 80% confidence intervals in Figure 5 shows a tendency of increasing uncertainty from the Near stack to the Ultra Far stack,

which is consistent with the user parametrized signal to noise ratios.

Figure 5 also shows some misalignment issues in the real seismic data, for example, around 5860 ms (orange rectangle). These misalignments impact the ISD algorithm (and any other independent deconvolution method) because it generates reflectivity spikes at different positions. These misalignments also impact the stability of the SSD solution: the amplitude of the reflectivity spikes is bigger for the Far and Ultra Far angle stacks, and they tend to present a dipole-like behavior aspect at the misaligned seismic events. On the other hand, the SSD algorithm still generates spikes at the same positions across all reflectivity stacks, and the Bayesian formalism tends to indicate bigger uncertainties where the input seismic is misaligned, which can be used as a quality control of the SSD algorithm.

Figure 6 compares ISD and SSD results on a real seismic line. The red boxes are visual aids to show the misalignment issues between Near and Ultra Far stacks. While the ISD spikes show the same misalignment

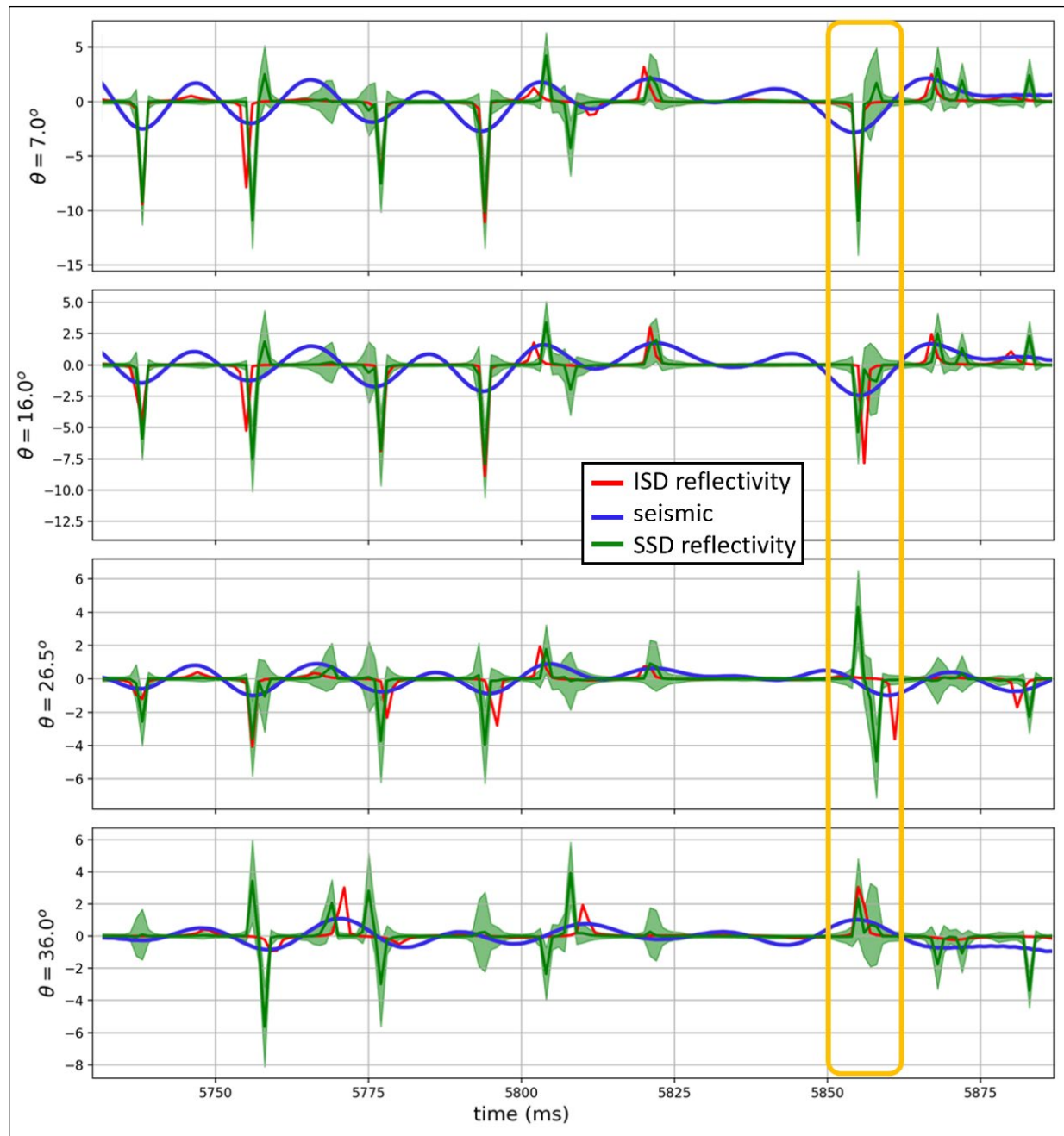


Figure 5: Result of the deconvolution on a single trace of the real seismic data. Orange rectangle shows the impact of seismic misalignment on the ISD and SSD algorithms.

issues present in the input seismic stacks, there is great structural conformity between Near and Ultra Far reflectivities obtained from SSD as can be seen from the sections.

CONCLUSIONS

The presented SSD (Simultaneous Sparse Deconvolution) technique developed here is based on the ARD formalism, together with a specific structure in the prior precision matrix, which couples the sparsity of different reflectivity traces. It has been shown, both

in synthetic and real case examples, that the SSD technique generates co-localized spikes, consequently resulting in more accurate results and better correlation between the resulting reflectivity traces.

Also, it has been shown that the SSD technique solves satisfactorily the misalignment due to different resolutions of the partial stacks, as illustrated in the synthetic example. On the other hand, more intense misalignment (due to residual moveout as illustrated in the real dataset) also impacts SSD, resulting in more unstable solutions, and dipole-like behavior in the reflectivity traces.

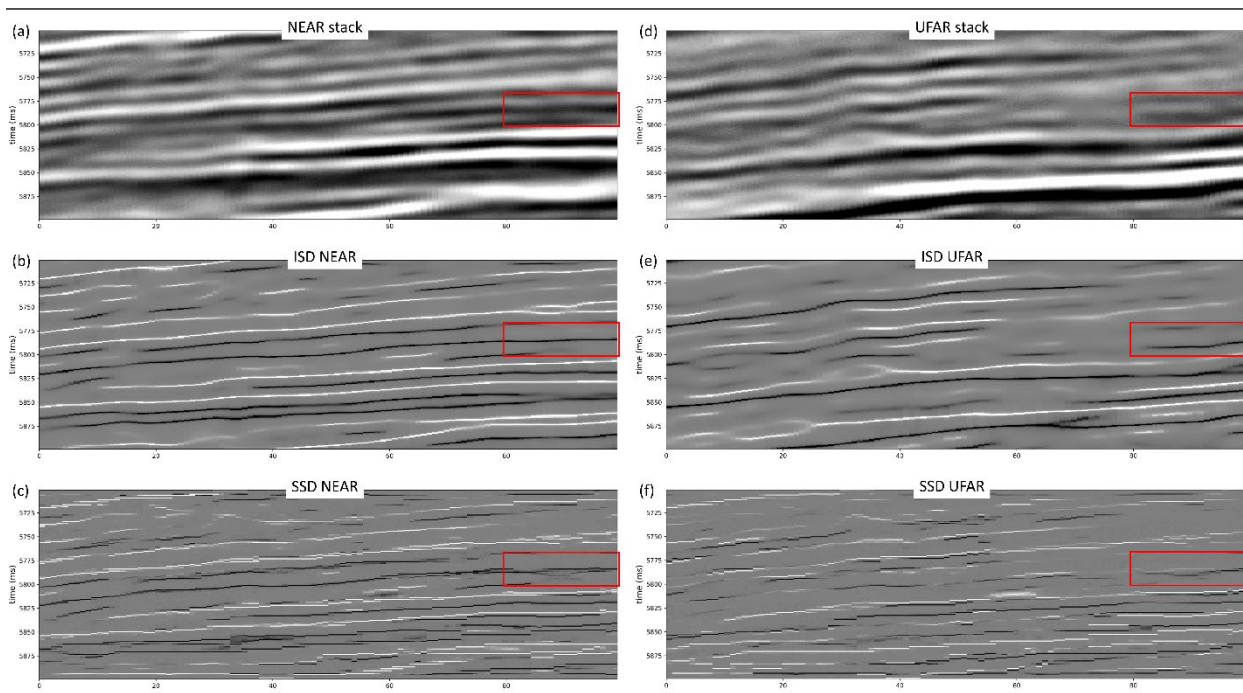


Figure 6: (a) Near seismic stack. (b) Near reflectivity computed from ISD. (c) Near reflectivity computed from SSD. (d) Ultra Far seismic stack. (e) Ultra Far reflectivity computed from ISD. (f) Ultra Far reflectivity computed from SSD

Finally, other types of seismic multi-stack inversion, such as elastic inversion, may benefit from the regularization technique presented in this paper.

ACKNOWLEDGMENTS

The authors would like to acknowledge Petrobras for the support and permission to publish the present work.

REFERENCES

- Bishop, C., 2006, *Pattern Recognition and Machine Learning*: Springer, New York, 738 pp. ISBN-10: 0387310738.
- Buland, A., and H. Omre, 2003, Bayesian linearized AVO inversion: *Geophysics*, **68**, 1, 185–198, doi: [10.1190/1.1543206](https://doi.org/10.1190/1.1543206)
- Cunha, C. A., L. T. Silva, N.S.M. Cruz, A. Damasceno, A. Pimentel, T. S. Oliveira, and A. Pimentel, 2019, High Resolution Impedance Inversion: *Brazilian Journal of Geophysics*, **37**, 4, 461–469, doi: [10.22564/rbgf.v37i4.2022](https://doi.org/10.22564/rbgf.v37i4.2022).
- Hargreaves, N., S. Treitel, and M. Smith, 2013, Frequency extension, resolution, and sparse inversion: *SEG Technical Program Expanded Abstracts 2013*, 3345–3349, doi: [10.1190/segam2013-0782.1](https://doi.org/10.1190/segam2013-0782.1)
- Lyche, T., 2020, The Kronecker Product, *in: Numerical Linear Algebra and Matrix Factorizations. Texts in Computational Science and Engineering*, **22**, Springer, Cham, 225–236, doi: [10.1007/978-3-030-36468-7_10](https://doi.org/10.1007/978-3-030-36468-7_10).
- Kazemi, N., and M. D. Sacchi, 2014, Sparse multichannel blind deconvolution: *Geophysics*, **79**, 5, V143–V152, doi: [10.1190/geo2013-0465.1](https://doi.org/10.1190/geo2013-0465.1).
- Rosa, A. L. R., 2018, *The seismic signal and its meaning*: Society of Exploration Geophysics, Geophysical References Series, **23**, 788 pp, doi: [10.1190/1.9781560803348](https://doi.org/10.1190/1.9781560803348).
- Valentine, A. and M. Sambridge, 2018, Optimal regularization for a class of linear inverse problem: *Geophysical Journal International*, **215**, 2, 1003–1021, doi: [10.1093/gji/ggy303](https://doi.org/10.1093/gji/ggy303).
- Ji, Y., H. Hu, Z. Lin, K. Zhang, and H. Zhong, 2020, The preconditioned ARD-based AVA inversion method for P-impedance and S-impedance: *SEG Technical Program Expanded Abstracts*, 355–359, doi: [10.1190/segam2020-3415458.1](https://doi.org/10.1190/segam2020-3415458.1)
- Sheriff, R. E., 1991, *Encyclopedic Dictionary of Exploration Geophysics*, 3rd ed., SEG, 376 pp.
- Xi, Y., X. Yin, and Z. Zong, 2018, AVO multi-trace group sparse inversion: *SEG Technical Program Expanded Abstracts*, 481–485, doi: [10.1190/segam2018-2995959.1](https://doi.org/10.1190/segam2018-2995959.1)

TALARICO, E.C.S.: developed the technique, applied it to the synthetic and real data, and analyzed the results; **SOBREIRA, M.C.A.:** participated on the method development discussions and application on the synthetic and real data and analysis of the results; **ARAUJO, A.G.:** preprocessed the real dataset and participated on the method application discussions and analysis of the results; **CUNHA FILHO, C.A.:** participated on the method development discussions and application on the synthetic and real data and analysis of the results.

Received on December 31, 2021 / Accepted on September 12, 2022